HHS Public Access

Author manuscript

Ann Neurol. Author manuscript; available in PMC 2018 May 09.

Published in final edited form as:

Ann Neurol. 2017 May ; 81(5): 690–702. doi:10.1002/ana.24930.

A mutation in the *Tubb4a* gene leads to microtubule accumulation with hypomyelination and demyelination

Ian D. Duncan, BVMS, PhD, FRCPath, FRSE[1,*], **Marianna Bugiani, MD, PhD**[5,6], **Abigail B. Radcliff, DVM**[1], **John J. Moran, BS**[4], **Camila Lopez-Anido, PhD**[4], **Phu Duong, BS**[4], **Benjamin K. August, BS**[3], **Nicole I. Wolf, MD, PhD**[6,7], **Marjo S. van der Knaap, MD, PhD**[6,7,8], and **John Svaren, PhD**[2,4]

[1]Department of Medical Sciences, School of Veterinary Medicine, University of Wisconsin-Madison, Madison, WI 53706, USA [2]Department of Comparative Biosciences, School of Veterinary Medicine, University of Wisconsin-Madison, Madison, WI 53706, USA [3]Electron Microscope Facility, School of Medicine and Public Health, University of Wisconsin-Madison, Madison, WI 53706, USA [4]Waisman Center, University of Wisconsin-Madison, Madison, WI 53705, USA [5]Department of Pathology, VU University Medical Center, Amsterdam, The Netherlands [6]Center for Childhood White Matter Disorders, Amsterdam Neuroscience, VU University Medical Center, Amsterdam, The Netherlands [7]Department of Child Neurology, VU University Medical Center, Amsterdam, The Netherlands [8]Department of Functional Genomics, Center for Neurogenomics and Cognitive Research, Amsterdam Neuroscience, VU University, Amsterdam, The Netherlands

Abstract

Objective—Our goal was to define the genetic cause of the profound hypomyelination in the *taiep* rat model and determine its relevance to human white matter disease.

Methods—Based on previous localization of the *taiep* mutation to rat chromosome 9, we tested if the mutation resided within the *Tubb4a* (β-tubulin 4A) gene, since mutations in the *TUBB4A* gene have been described in patients with CNS hypomyelination. To determine whether accumulation of microtubules led to progressive demyelination we analyzed the spinal cord and optic nerves of 2 year old rats by light and electron microscopy. Cerebral white matter from a patient with *TUBB4A* Asn414Lys mutation and MRI evidence of severe hypomyelination was studied similarly.

Results—As the *taiep* rat ages there is progressive loss of myelin in the brain and dorsal column of the spinal cord associated with increased oligodendrocyte numbers with accumulation of microtubules. This accumulation involved the entire cell body and distal processes of oligodendrocytes but there was no accumulation of microtubules in axons. A single point mutation

Corresponding author: Ian D. Duncan, 2015 Linden Drive, Madison, WI 53706. Phone: 608-263-9828, Fax: 608-265-8020., ian.duncan@wisc.edu.

AUTHOR CONTRIBUTIONS:

I.D.D. and J.S. contributed to study concept and design. All authors contributed to data acquisition and analysis. I.D.D., A.B.R., C.L-A., P.D., M.B., M.S. vdK., J.S. contributed to drafting the text or preparing the figures.

POTENTIAL CONFLICTS OF INTEREST:

None of the authors have any conflict of interest.

in *Tubb4a* (p.Ala302Thr) was found in homozygous *taiep* samples. A similar hypomyelination associated with increased oligodendrocyte numbers and arrays of microtubules in oligodendrocytes was demonstrated in the human patient sample.

Interpretation—The *taiep* rat is the first animal model of *TUBB4* mutations in humans and a novel system in which to test the mechanism of microtubule accumulation. The finding of microtubule accumulation in a patient with a *TUBB4A* mutation and leukodystrophy confirms the usefulness of *taiep* as a model of the human disease.

Keywords

Hypomyelination; demyelination; microtubules; *Tubb4a* gene; leukodystrophy

INTRODUCTION

Hypomyelination with atrophy of the basal ganglia and cerebellum (H-ABC) is a rare childhood leukodystrophy first described by van der Knaap, Naidu [1]. Patients with the disease have extrapyramidal movement abnormalities, spasticity, cerebellar ataxia and sometimes epilepsy[1, 2]. Diagnosis of H-ABC is made principally by MRI showing marked atrophy or disappearance of the putamen, along with atrophy of the caudate nucleus, cerebellar atrophy and hypomyelination being regarded as the cardinal diagnostic criteria. In addition, progressive loss of myelin is seen in most patients on serial MRI[2–4].

H-ABC is a rare disorder which has been demonstrated to be inherited as a dominant *de novo* mutation in *TUBB4A*[2, 4–6]. *TUBB4A* encodes β-tubulin, which dimerizes with α-tubulin as the major subunits of microtubules. *TUBB4A* is expressed predominately in the brain, and recent cell type-specific expression profiling has identified *Tubb4a* as highly expressed in oligodendrocytes compared to neurons, astrocytes, and microglia [7]. Since the identification of *TUBB4A* mutations in H-ABC, *TUBB4A* mutations has been associated with a spectrum of disease symptoms that vary in serverity[8]. On the mildest end is adult onset DYT4 dystonia or whispering dysphonia, characterized by extrapyramidal movement abnormalities without any white matter abnormalities on MRI. The second disease phenotype in order of severity is mild, isolated hypomyelination. Other phenotypes include classical H-ABC and severe isolated hypomyelination with variable cerebellar atrophy and clinically a devastating encephalopathy[2, 8].

At present it is hypothesized that in H-ABC a microtubule defect resulting from the *TUBB4A* mutations primarily affects axons with secondary effects on glia resulting in the myelin sheath changes[5]. It is possible that the cell type primarily affected could be dependent upon specific mutations of *TUBB4A*. Models that could be used to explore the effects of these mutations on axons and glia until now are lacking. A potential model of *TUBB4A*-related disease is the myelin mutant rat, called *taiep*[9]. This rat develops a progressive neurologic disease resulting from hypomyelination followed by demyelination of the brain, optic nerves and certain tracts of the spinal cord[10, 11]. Progressive accumulation of microtubules in oligodendrocytes was correlated with failure to develop normal myelin (hypomyelination) and subsequent demyelination[12]. We previously mapped the *taiep* mutation to a 5–9 cM region around *D9Rat44* of rat chromosome 9[13]. We have now

identified a mutation in *Tubb4a* in the *taiep* rat in an amino acid that is located in a domain involved in interactions between the α- and β-tubulin dimers. Thus, *taiep* is an ideal model in which to study the mechanism of microtubule accumulation in the oligodendrocyte cell body and throughout its processes.

MATERIALS AND METHODS

Animals

All animal experiments were performed according to protocols approved by the University of Wisconsin School of Veterinary Medicine Institutional Animal Care and Use Committee. The *taiep* rat colony was maintained by the crossing of affected x affected rats or affected x carrier rats of either sex. Offspring resulting from carrier x affected pairings were differentiated by the development of a tremor in affected pups around 20 days of age[10]. Affected *taiep* rats were able to live up to 27 months of age with supportive animal care.

Myelin stain of the brain

As previously described[12], we used a simple histochemical stain on 40 μm free floating sections stained with nitroblue tetrazolium and diaminobenzidine[14].

Light microscopy and electron microscopy (EM)

Affected *taiep* rats, heterozygotes and age-matched normal littermates were perfused with a modified Karnovsky fixative as previously described[15]. Following perfusion, the brain, optic nerves and whole spinal cord were removed-and post-fixed for at least two days; then blocks were trimmed for processing and plastic embedding. These were cut as detailed previously[10] for light and electron microscopy (EM) and viewed on a Philips CM120 transmission electron microscope. Images were captured with a Software BioSprint 12 series digital camera using AMT Image Capture Software Engine V700.

Neuropathology of the brain

Brains from *taiep* rats and age-matched controls at 2 weeks, 3 months, 1 year and 2 years (two at each time point) were collected following perfusion, as described above. The brains were trimmed, processed and embedded in paraffin. Coronal sections were stained with hematoxylin and eosin (H&E), luxol fast blue/PAS and cresyl violet.

Mutation identification and validation

RNA was isolated from *taiep* (n=2) and control (n=2) rat spinal cord samples via Trizol extraction. This was converted to cDNA using oligo$(dT)_{20}$ primer (IDT) and MMLV reverse transcriptase (Invitrogen). Sequencing reactions were then prepared using 2ng of cDNA template and one of the following four sequencing primers spanning the ~1500 bp *Tubb4a* ORF:

F1: ATCTCCTCCAGAGACGGAACCAC; F2: CCACCTAGTGTCGGCCACCAT

R1: ACACCAGCAAATCTTTGACCCTG; R2: CTCAATGCAGATCTACGCAAGC

Sequencing of affected *taiep* rat cDNA indicated the presence of a SNP that generated a novel MscI restriction site. This was validated by PCR using primers F1 and R1 (above) to produce a product 1460bp long followed by digestion with MscI (NEB). The control PCR fragment contained one MscI site at 318bp, and the *taiep* PCR fragment added an additional site at 804bp. Therefore, the digest band sizes expected for each condition were as follows: Control: 318, and 1142bp; *taiep*: 318, 486, and 656bp.

Genotyping primers with the following sequences were designed to span the novel *taiep* SNP site:

F: GAGAACACTGATGAGACCTACTG; R: CCTGGATGGCTGTGCTATT

PCR with rat gDNA produced a product of 547bp. Subsequent digestion with MscI was expected to produce band sizes as follows: Control: 547bp; *taiep*: 225, 322bp; Het: 225, 322, 547bp. The *Tubb4a* mutations were modeled on the *Tubb3* structure[16] using PyMOL(TM) Molecular Graphics System, Version 1.7.1.4.

ChIP-qPCR

ChIP assays were performed on pooled thoracic spinal cords from postnatal day 15 (P15) C57BL/6 mice using the following antibodies: goat IgG (Santa Cruz Biotechnology, sc-2028), Sox10 (R&D, AF2864), and Olig2 (Millipore, AB9610). ChIP-qPCR was performed as described previously[17, 18] on three independent experiments, and primers used will be provided on request. P-values were obtained from the Student's two-tailed t test to compare percent recoveries in Sox10 or Olig2 ChIP assays compared with that in a control IP (goat IgG) ($p < 0.05$ is considered to be statistically significant).

Patient light microscopy and EM

A patient with severe hypomyelination and clinically, a profound lack of development, died at the age of almost 4 years because of respiratory failure. This patient harbored a *de novo TUBB4A* gene mutation, c.1242C>G / p.Asn414Lys, not present in the parents, in line with dominant *de novo* inheritance.

Post-mortem tissue was formalin-fixed paraffin-embedded for (immuno)histochemistry. Four-μm-thick tissue sections were stained with H&E, Klüver stain for myelin and Bodian stain for axons according to standard methods. After heat-induced antigen retrieval in 0.01M citrate buffer (pH6), immunohistochemical staining was performed with antibodies against the major myelin protein proteolipid protein (PLP; AbDserotec, 1:3000), the astrocyte-specific protein glial fibrillary acidic protein (GFAP; Millipore, 1:1000), and CD68 for microglia (Dako, clone KP1, 1:400). Immunoreactivity was detected with 3,30-diaminobenzidine as a chromogen. Tissue sections were photographed using a Leica DM6000B microscope (Leica Microsystems). Omitting primary antibodies yielded no significant staining.

EM was performed on frontal white matter. The tissue was fixed with 2% glutaraldehyde in 0.1M sodium cacodylate buffer (pH 7.4), post-fixed in 2% osmium tetroxide and embedded in epoxy resin. Ultrathin sections were stained with uranyl acetate and lead citrate.

RESULTS

1) *taiep* rat phenotype

As previously described, the *taiep* rat develops a tremor at 15–20 days of age involving the trunk and limbs[9]. This is not lethal and *taiep* rats can frequently live up to 2 years of age and beyond, i.e. a normal rat lifespan. While they develop a progressive neurologic disease from around 3 months on, this usually plateaus at 12–15 months with persistent truncal ataxia, paresis and intermittent seizure activity. Despite severe involvement of the optic nerves, vision most often remains intact. Both male and female carriers that live up to two years of age show no neurological abnormalities.

2) Myelin development and loss in the *taiep* brain and brain neuropathology

Gross examination of the sagittally sectioned brain at early time points (2–3 months), showed that myelin was present in the major white matter tracts (e.g. cerebellar medulla and folia and the corpus callosum), but was not as obvious as in control rats. This was confirmed in sections stained with the simple myelin stain[14] which showed some myelin in the brain stem and forebrain (Fig. 1), but much less than normal. By 9–12 months, however, a total loss of myelin in *taiep* was observed throughout the brain (Fig. 1).

The major abnormalities seen in the *taiep* brain sections were the initial paucity of myelin followed by a generalized loss of myelin associated with enlargement of the ventricles, consistent with progressive white matter atrophy. There was no evidence of atrophy of the basal ganglia, including the putamen and caudate nucleus, though the cerebellum showed a mild decrease in size but without clear neuronal loss.

3) Myelin development and loss in the spinal cord in the *taiep* rat

At the early time points (2–3 months) there was a striking hypomyelination of the spinal cord with axons in all columns of the cord being thinly myelinated or lacking a myelin sheath, especially the dorsal column (Fig. 2D, E). Some large diameter axons appeared to have a myelin sheath of normal thickness (Fig. 2E). In the dorsal column, the fasciculus gracilis and corticospinal tracts, which contain mainly small caliber axons, were uniformly hypomyelinated at early time points (Fig. 2E). By 6–9 months, these tracts lost practically all myelin and contained predominantly demyelinated axons (Fig. 2G, H). There was a striking increase in oligodendrocytes in these tracts despite the loss of myelin (Fig. 2H). In the ventral column, hypomyelination persisted throughout life though many scattered fibers had thick myelin sheaths (Fig. 2F, I). No myelin abnormality was seen in the spinal cord of heterozygote rats up to 16 months of age.

4) Oligodendrocyte abnormality in the *taiep* rat

The hallmark abnormality was the progressive accumulation of microtubules throughout the oligodendrocyte cell body and its processes (Fig. 3). This accumulation was not apparent prior to the onset of myelination in the postnatal day 7 (P7) *taiep* optic nerve. However, it was present in the P7 spinal cord of the same rat, where there was active myelination. Microtubules increased initially in a scattered fashion throughout the cytosol, then were seen in linear rows, either alone or with a predisposition to align along elements of the

endoplasmic reticulum (ER) and the outer nuclear envelope (Fig. 3B, C, F). This ER had the appearance of smooth ER, or transitional elements[19] as it lacked ribosomes. These accumulations persisted in oligodendrocytes for up to two years of age. Microtubule accumulation was also seen in large and fine oligodendrocyte processes throughout the neuropil and to the furthest point of the cell process in the outer and inner oligodendrocyte cytoplasmic loops (Fig. 3H). Collections of small oligodendrocyte processes that were packed with microtubules were seen throughout the neuropil, though often adjacent to oligodendrocyte cell bodies (Fig. 3H, I). In some cases, microtubules were seen in excess number encircling a myelinated axon (Fig. 3G). Microtubules were occasionally aligned on the rough ER where they may have displaced ribosomes, and on the outer nuclear membrane (Fig. 3D, E). In older *taiep* rats, densely packed microtubules were found throughout the cytosol to the exclusion of other organelles. Microtubule accumulation was limited to the oligodendrocyte cell body and its processes and was never seen in adjacent axons that had a normal microtubule density (Fig. 3I). Likewise, there was no evidence of microtubule accumulation in astrocytes.

5) Mutation in the *taiep* rat and gene regulation analyses

Previous gene mapping studies of the *taiep* rat had localized the gene to chromosome 9, between D9Rat88 marker and the telomere, which is approximately a 12 Mb segment in the Rn5 genome[13]. A survey of genes in this interval revealed that the *Tubb4a* gene for β4 tubulin resided there, and expression profiles have shown that *Tubb4a* is highly expressed in newly formed and myelinating oligodendrocytes, but much lower in oligodendrocyte progenitor cells (OPCs) and other CNS cell types[7]. Other profiling studies also indicate oligodendrocyte specific expression[20]. We initially examined levels of *Tubb4a* in both *taiep* and littermate rats, and saw only minimal differences in gene expression by qRT-PCR (data not shown). Rat spinal cord cDNA was prepared from homozygous *taiep* and wild type littermates, and the open reading frame (ORF) was amplified and sequenced. The length of the ORF as determined by PCR was unchanged in *taiep* relative to wild type littermate. The sequencing revealed a single coding mutation that converted Ala302 to Thr (GCG to ACG) in the homozygous *taiep* samples (Fig. 4A). The sequence change also introduces a restriction site, MscI, which was used to validate the sequence change after digestion of the PCR products from the cDNA.

The Ala302 mutation is located in a domain proposed to mediate lateral interactions between αβ-tubulin heterodimer units, which assemble to form cylindrical microtubules[21] (Fig. 4B). The closest *TUBB4A* mutation identified in H-ABC was p.Gln292Lys[22], although one of the *TUBB3* mutations associated with a nervous system disorder with axon guidance defects was the homologous p.Ala302Thr mutation[23], discussed below. Together with the previous evidence of accumulation of microtubules in *taiep* oligodendrocytes, we concluded that this is likely to be the responsible mutation.

To address how *Tubb4a* gene expression is controlled in oligodendrocytes, we hypothesized that it may be directly regulated by the critical oligodendrocyte transcription factors Sox10 and Olig2[24–26]. Our Sox10 ChIP-Seq dataset[18, 27] from P15 rat thoracic spinal cord indicated that Sox10 may bind a genomic region about −8kb upstream of the *Tubb4a* TSS,

as well as the gene promoter. Sequence analysis revealed a Sox10 binding motif at the promoter, but the motif appears to be poorly conserved in humans (Fig. 5A). In addition, the Olig2 binding motif was found at the promoter and the genomic region at −8kb, albeit the motif at −8kb is also not conserved in humans.

We next hypothesized that Olig2 binding may be a conserved regulatory event at the *Tubb4a* promoter. To test this and validate cross-species conservation, ChIP-qPCR was performed on P15 mouse thoracic spinal cords with antibodies for Sox10 or Olig2. Indeed, we found that Olig2 binds the *Tubb4a* promoter and −8kb sites, though not as strongly at the latter (Fig. 5B). Sox10 was also found to significantly bind the gene promoter, but the percent recovery was not as high as was seen for the positive control. As a positive control, we detected Sox10 and Olig2 binding at a known regulatory element at −27kb upstream of the *Sox10* gene (*Sox10-MCS4/U3*)[28]. No binding was detected at a negative control site near *Tektin 3* (*Tekt3*), a testes-specific gene. Our results indicate that Sox10 and Olig2 bind the *Tubb4a* promoter and directly regulate expression of *Tubb4a* in oligodendrocytes.

To further examine regulation of *Tubb4a* gene expression by Sox10 and Olig2, we mined a previous transcriptomics analysis on *Brg1*-deficient oligodendrocytes from optic nerve[29], as both Olig2 and Sox10 interact with Brg1[29, 30]. Optic nerve from P14 *Brg1* cKO (*Brg1*$^{flox/flox}$; *Olig1*-Cre) mice exhibits myelination defects, as well as reduced levels of *Sox10* (>4-fold) and *Olig2* (>3-fold)[29]. *Tubb4a* gene expression is also downregulated >5-fold in *Brg1* cKO optic nerve. Olig1 is co-expressed with Olig2 and is required for oligodendrocyte differentiation[24]. *Olig1* expression is also reduced in *Brg1* cKO nerve[29] and Olig1-deficient optic nerve exhibits reduced Tubb4a levels[31], providing further evidence that *Tubb4a* is regulated by oligodendrocyte specific transcription factors.

6) Light microscopy and EM in the human patient

To determine if the microtubule accumulation seen in the *taiep* rat was observed in a human patient with a *TUBB4A* mutation, we analyzed samples from a 2½ year old patient with a p.Asn414Lys mutation. This patient had profound hypomyelination and mild cerebellar atrophy, without atrophy of the putamen and caudate nucleus (Fig. 6). The mutation was located in the H12 helix domain (Fig. 4B), which is involved in contacts with microtubule-associated proteins and kinesin motors[21, 32].

On macroscopic brain examination, the deep and subcortical white matter in the cerebral lobes, as well as in the internal capsule, anterior commissure and corpus callosum was discolored and undiscernible from the neighboring gray matter. The lateral ventricles were enlarged and the corpus callosum thin, indicating white matter atrophy. On coronal cut, the putamen and caudate nucleus had a normal appearance. The cerebellum was moderately atrophic, especially the vermis. On microscopic examination, the white matter of the deeper and subcortical cerebral areas showed a marked lack of myelin (Fig. 7A, B). At high magnification, microscopy revealed increased density of white matter oligodendrocytes, without axonal swellings or spheroids (Fig. 7C). The lack of myelin was conceivably due to both hypomyelination and myelin degeneration, as scattered macrophages could be focally seen in perivascular regions (Fig. 7D). The axons were much better preserved (Fig. 7E). In the white matter, immunohistochemistry demonstrated activation of microglia and

isomorphic reactive astrogliosis (Fig. 7F). The cerebral cortex was normal. The putamen and caudate nucleus were, like the thalamus and globus pallidus, intact. The cerebellar cortex was atrophic with loss of neurons in the granular layer (Fig. 7G). The molecular layer was thinned and mildly gliotic. There was only a minor loss of Purkinje cells, but the remaining Purkinje cells showed swollen dendrites and axons (Fig. 7H). The cerebellar white matter was pale.

EM of the white matter showed marked hypomyelination with most axons being thinly myelinated (Fig. 8A). Many large diameter axons lacked a myelin sheath. Oligodendrocytes were present, more than normal, and within these there was evidence of an increase of microtubules, often seen in longitudinal arrays (Fig. 8B, C). Many oligodendrocyte inner loops were enlarged with increased microtubules (Fig. 8D, E) and longitudinal processes of oligodendrocytes contained prominent microtubules (Fig. 8F). Microtubules were also noted to be increased in some axons (Fig. 8G), but there was no evidence of accumulation of other organelles, spheroids or axon degeneration.

DISCUSSION

Since 2002, there has been a growing number of reports of mutations in the *TUBB4A* gene associated with variable phenotypes ranging from severe early onset fatal encephalopathy with profound lack of myelin to milder disease characterized by milder or no myelin deficits. While in classical H-ABC atrophy of the putamen is obligatory[1, 3], both severe and milder hypomyelinating variants without atrophy of the putamen and caudate nucleus have been observed[2, 8]. The lack of tissue from affected patients has left gaps in our understanding of H-ABC and other *TUBB4A*-related phenotypes, of the development of changes in the basal ganglia as well as the defects in myelin production and maintenance. Here we present a rat mutant with a mutation in *Tubb4a* that has a profound disturbance of myelin caused by an abnormality of microtubules in oligodendrocytes resulting in hypomyelination and subsequent demyelination, which might model the changes in *TUBB4A*-related hypomyelination and identify the primary target cell.

Microtubules are essential structures of the developing CNS, playing a major role in neuronal migration and axonal guidance[33]. The tubulin gene family comprises a large number of genes that encode two dimeric proteins, α and β tubulin that form microtubules. Mutations of these genes, including *TUBA1A*, *TUBA8*, *TUBB2B* and *TUBB3* that encode neuronal microtubules, result in CNS malformations such as cortical malformations and defects in commissural fiber tracts[23]. Microtubules are also important constituents in oligodendrocytes where with actin they form the major components of the cell cytoskeleton[34, 35], and play an essential role in trafficking of certain myelin proteins and mRNAs[36–38]. Mutations in *TUBB4A* result in a disease spectrum, ranging from adult onset dystonia type 4 (DYT4), also called whispering dysphonia, to isolated mild hypomyelination, H-ABC of variable severity, and isolated severe hypomyelination[2, 8]. The diagnosis of H-ABC is made in life by the MRI triad of atrophy of the putamen, atrophy of the cerebellum and hypomyelination[1, 2, 4]. However, patients without atrophy of the putamen have been reported more recently[4, 22, 39] and indeed there appears to be a broad spectrum of presentations[8]. All reported patients have heterozygous dominant mutations. The enigma of

H-ABC, however, is why severe atrophy of the putamen coexists with hypomyelination, two very different processes that appear unrelated[1].

Accumulation of microtubules in *taiep* oligodendrocytes initially appears randomly throughout the cell body, but then microtubules align with apparent smooth ER profiles, either partially or completely coating the surface. There also appears to be an alignment of free microtubules in the cell cytosol, with microtubules often arranged in linear rows. Microtubule accumulation is seen throughout cell processes and their extensions into the inner and outer cytoplasmic loops of the myelin sheath. Microtubules less frequently were aligned along the outer nuclear envelope and also its extension, rough ER, with displacement of ribosomes. Another striking cellular feature of the white matter in the mutant rat is the frequent presence of microprocesses that increase with aging. These contain densely packed microtubules and are therefore thought to be small caliber oligodendrocyte processes. Similar microprocesses have been described in the *shiverer* (*shi*) mouse[40]. In the *taiep* rat spinal cord dorsal column, as in the brain white matter of our patient with *TUBB4A*-related severe hypomyelination, there is an increase of oligodendrocyte nuclei often associated with bundles of microprocesses (data not shown) that might suggest a failure of oligodendrocyte maturation.

While it is not known why the *taiep* mutation results in preferential loss of myelin in the fasciculus gracilis and corticospinal tracts, oligodendrocytes in these tracts myelinate primarily small diameter axons. We have previously shown that such oligodendrocytes in the *taiep* anterior medullary velum (AMV) are also preferentially involved over those myelinating large axons[41]. The AMV is a thin structure that lies between the cerebellum and inferior colliculi in which oligodendrocytes myelinating large and small axons can be separately visualized[42]. Likewise, in the brain parenchyma and optic nerves, oligodendrocytes that myelinate small to medium diameter axons are preferentially involved. Hence demyelination in the brain is more severe than in the lateral and ventral columns of the spinal cord where oligodendrocytes myelinate larger diameter axons. Accordingly, the polarity of microtubules in fine processes of oligodendrocytes is disrupted more than in large diameter processes that may myelinate larger caliber axons[43].

The *taiep* microtubule accumulation and alignment with cytosolic membranes appears to be a unique observation compared to other white matter disorders. The microtubular defect in the *taiep rat* does, however, have a striking resemblance to that seen experimentally in both CNS cultures and in Schwann cells after exposure to taxol. In organotypic mouse spinal cord-dorsal root ganglion cultures, six day exposure to taxol resulted in marked increase in microtubules in oligodendrocytes and their association with ER cisternae and the outer nuclear envelope[44]. The location of the taxol-binding site on microtubules is known[45], thus the taxol model might shed light on apparent identical microtubule changes seen in *taiep* and, putatively, *TUBB4A*-related disorders.

The comparison with *TUBB3* mutations provides a number of interesting points. For example, *TUBB3* mutations cause neuronal migration defects[46], whereas the analysis here and previously highlights a significant defect mainly in *TUBB4A* mutant oligodendrocytes. Accordingly, *TUBB4A* is highly expressed in newly formed and myelinating

oligodendrocytes, relative to OPCs and neurons, while the *TUBB3* gene is specifically expressed in neurons[7]. The regulation of *TUBB4A* by Olig2 and Sox10 is also consistent with this idea. Interestingly, the *taiep* mutation does not cause myelin changes in peripheral nerve where other tubulin genes are expressed highly (e.g. *Tubb2a, Tubb4b*, and *Tubb5*). Likewise, patients with H-ABC also do not have a peripheral neuropathy. Another important similarity is that human mutations in *TUBB3* and *TUBB4A* are generally heterozygous. However, no phenotype is observed in heterozygous *taiep* rats. Similarly, a *Tubb3* knockin mutation was generated previously and showed a phenotype only in the homozygous state[46]. We do not know the reasons for the requirement of homozygosity, but the microtubule dynamics in rodents may render them less sensitive to expression of mutant tubulin protein. Alternatively, it is possible that the lack of a phenotype in the heterozygous mutant may be due to relatively short lifespan of the rat. The genetic differences between these mutations in rat and human may be comparable to another leukodystrophy, vanishing white matter, which in humans has a recessive inheritance with mutations in either of the 5 genes *EIF2B1-5*. Mutations that lead to a childhood disease in humans, give at most a very mild phenotype in mice[47]. Only severe mutations and especially double mutants with mutations in two genes give an adequate neurological phenotype in mice[48].

Finally, the TUBB4A protein is highly related to the TUBB3 protein. A recent study employed the homologous mutation (*Tubb3* Ala302Thr) in a yeast analysis of microtubule dynamics and found that the mutation made microtubules more stable, and the mutant protein had reduced dynamics of polymerization/depolymerization[46]. Interestingly, the *TUBB4A* mutation in our patient at Asn414 affects the H12 domain which interacts with kinesin motors and other microtubule-associated proteins[32, 49] (Fig. 4B). In addition, a nearby mutation at position 417 in TUBB3 reduces kinesin binding and leads to increased polymerization and higher stability of microtubules[16]. Therefore, studies of similar mutations in TUBB3 suggest that mutations at Ala302 in the *taiep* rat and at Asn414 in the patient described here both cause enhanced stability of microtubules could lead to the observed accumulation of microtubules. Other *TUBB4A* mutations associated with the H-ABC phenotype or hypomyelination affect amino acids at the α-β-tubulin interface (2), or domains that mediate interactions between protofilaments that form the microtubules or affect microtubule function. Therefore, different *TUBB4A* mutations have different downstream molecular effects that underlie the diverse *TUBB4A*-related phenotypes.

Microtubules exhibit dynamic instability, involving the stochastic polymerization and depolymerization from their plus end[50, 51]. We hypothesized that the increased density of microtubules in *taiep* oligodendrocyte processes resulted in an imbalance in kinesin/dynein activity resulting in the decreased transport of MBP mRNA granules and myelin-specific proteins toward the distal end of oligodendrocyte processes[12, 52]. In addition, microtubule polarity, which is inherently plus end distal in oligodendrocyte processes[38], is abnormal in *taiep* with a mix of plus and minus end distal tubules in fine oligodendrocyte processes[43]. The molecular pathogenesis of *Tubb4a* mutations has not been established and the *taiep* rat model provides an ideal tool in which to address this question.

Can the *taiep* rat therefore model the phenotype of *TUBB4A* mutations in humans and provide a mechanism for the myelin and possibly neuronal disorder? The *taiep* rat shows a

clear and consistent phenotype with hypomyelination followed by demyelination of the brain. This is strikingly similar to what is thought to occur in H-ABC and *TUBB4A*-related hypomyelination variants as observed by MRI[2, 4]. The microtubule defect, however, is restricted to oligodendrocytes in *taiep*, with no evidence of their accumulation in axons. The myelin defect is much more pronounced in the brain of the *taiep* rat than in the spinal cord where more myelin is seen, albeit with hypomyelination and where demyelination only affects certain tracts of the dorsal column. There is no atrophy of the putamen in *taiep* rats yet the cerebellum is smaller and there is a separation of the gyri, which suggests atrophy. However, there was no histologic evidence of loss of neurons in the cerebellum, and the mild reduction in size may result from myelin loss. Thus the *taiep* rat has greatest similarity to those *TUBB4A*-mutated patients who have severe isolated hypomyelination. The finding of microtubule accumulation in the patient described here confirms the usefulness of the *taiep* rat as a model of *TUBB4A* mutations and provides a system in which to test therapies.

Acknowledgments

We dedicate this paper to the memory of Drs. Bjorn and Ruth Holmgren who identified the *taiep* mutation and had the intellectual curiosity and drive to maintain the colony and define its mode of inheritance. We are grateful to Drs. A. Gendron-Fitzpatrick and R. Salamat for the brain neuropathology studies and Dr. Erik Dent for his comments on the manuscript. The work was supported by the Boespflug Foundation (I.D.D.), and more recently The Foundation to Fight H-ABC (I.D.D.), NIH (NS075269 to J.S. and U54 HD090256 to the Waisman Center), and the Optimix Foundation for Scientific Research (M.S.v.d.K.).

References

1. van der Knaap MS, Naidu S, Pouwels PJ, et al. New syndrome characterized by hypomyelination with atrophy of the basal ganglia and cerebellum. AJNR Am J Neuroradiol. 2002 Oct; 23(9):1466–74. [PubMed: 12372733]
2. Hamilton EM, Polder E, Vanderver A, et al. Hypomyelination with atrophy of the basal ganglia and cerebellum: further delineation of the phenotype and genotype-phenotype correlation. Brain. 2014 Jul; 137(Pt 7):1921–30. [PubMed: 24785942]
3. van der Knaap MS, Linnankivi T, Paetau A, et al. Hypomyelination with atrophy of the basal ganglia and cerebellum: follow-up and pathology. Neurology. 2007 Jul 10; 69(2):166–71. [PubMed: 17620549]
4. Ferreira C, Poretti A, Cohen J, Hamosh A, Naidu S. Novel TUBB4A mutations and expansion of the neuroimaging phenotype of hypomyelination with atrophy of the basal ganglia and cerebellum (H-ABC). Am J Med Genet A. 2014 Jul; 164A(7):1802–7. [PubMed: 24706558]
5. Simons C, Wolf NI, McNeil N, et al. A de novo mutation in the beta-tubulin gene TUBB4A results in the leukoencephalopathy hypomyelination with atrophy of the basal ganglia and cerebellum. Am J Hum Genet. 2013 May 2; 92(5):767–73. [PubMed: 23582646]
6. Tonduti D, Aiello C, Renaldo F, et al. TUBB4A-related hypomyelinating leukodystrophy: New insights from a series of 12 patients. Eur J Paediatr Neurol. 2016 Mar; 20(2):323–30. [PubMed: 26643067]
7. Zhang Y, Chen K, Sloan SA, et al. An RNA-sequencing transcriptome and splicing database of glia, neurons, and vascular cells of the cerebral cortex. The Journal of neuroscience : the official journal of the Society for Neuroscience. 2014 Sep 3; 34(36):11929–47. [PubMed: 25186741]
8. Hamilton EM, Wolf NI, van der Knaap MS. Reply: TUBB4A novel mutation reinforces the genotype-phenotype correlation of hypomyelination with atrophy of the basal ganglia and cerebellum. Brain. 2015 Feb.138(Pt 2):e328. [PubMed: 25168211]
9. Holmgren B, Urba-Holmgren R, Riboni L, Vega-SaenzdeMiera EC. Sprague Dawley rat mutant with tremor, ataxia, tonic immobility episodes, pilepsy and paralysis. Lab Anim Sci. 1989; 39:226–8. [PubMed: 2724922]

10. Duncan ID, Lunn KF, Holmgren B, Urba-Holmgren R, Brignolo-Holmes L. The taiep rat: A myelin mutant with an associated oligodendrocyte microtubular defect. JNeurocytol. 1992; 21:870–84. [PubMed: 1469463]
11. Lunn KF, Clayton MK, Duncan ID. The temporal progression of the myelination defect in the taiep rat. JNeurocytol. 1997; 26:267–81. [PubMed: 9192292]
12. O'Connor LT, Goetz BD, Couve E, Song J, Duncan ID. Intracellular distribution of myelin protein gene products is altered in oligodendrocytes of the taiep rat. Mol Cell Neurosci. 2000; 16:396–407. [PubMed: 11085877]
13. Li FY, Song J, Duncan ID. Mapping of taiep rat phenotype to rat Chromosome 9. Mamm Genome. 2003 Oct; 14(10):703–5. [PubMed: 14694906]
14. Kaatz KW, Bazzett TJ, Albin RL. A new, simple myelin stain. Brain ResBull. 1992; 29:697–8.
15. Griffiths IR, Duncan ID, McCulloch M, Harvey MJA. Shaking pups: A disorder of central myelination in the Spaniel dog. I. Clinical, genetic and light microscopical observations. J Neurol Sci. 1981; 50:423–33. [PubMed: 7196438]
16. Ti SC, Pamula MC, Howes SC, et al. Mutations in human tubulin proximal to the kinesin-binding site alter dynamic instability at microtubule plus- and minus-ends. Dev Cell. 2016 Apr 4; 37(1): 72–84. [PubMed: 27046833]
17. Srinivasan R, Sun G, Keles S, et al. Genome-wide analysis of EGR2/SOX10 binding in myelinating peripheral nerve. Nucleic Acids Res. 2012 Aug; 40(14):6449–60. [PubMed: 22492709]
18. Lopez-Anido C, Sun G, Koenning M, et al. Differential Sox10 genomic occupancy in myelinating glia. Glia. 2015 May 14.
19. Couve E, Cabello JF, Krsulovic J, Roncagliolo M. Binding of microtubules to transitional elements in oligodendrocytes of the myelin mutant taiep rat. JNeurosciRes. 1997; 47:573–81.
20. Marques S, Zeisel A, Codeluppi S, et al. Oligodendrocyte heterogeneity in the mouse juvenile and adult central nervous system. Science. 2016 Jun 10; 352(6291):1326–9. [PubMed: 27284195]
21. Lowe J, Li H, Downing KH, Nogales E. Refined structure of alpha beta-tubulin at 3.5 A resolution. J Mol Biol. 2001 Nov 9; 313(5):1045–57. [PubMed: 11700061]
22. Pizzino A, Pierson TM, Guo Y, et al. TUBB4A de novo mutations cause isolated hypomyelination. Neurology. 2014 Sep 2; 83(10):898–902. [PubMed: 25085639]
23. Tischfield MA, Cederquist GY, Gupta ML Jr, Engle EC. Phenotypic spectrum of the tubulin-related disorders and functional implications of disease-causing mutations. Curr Opin Genet Dev. 2011 Jun; 21(3):286–94. [PubMed: 21292473]
24. Lu QR, Sun T, Zhu Z, et al. Common developmental requirement for Olig function indicates a motor neuron/oligodendrocyte connection. Cell. 2002 Apr 5; 109(1):75–86. [PubMed: 11955448]
25. Stolt CC, Rehberg S, Ader M, et al. Terminal differentiation of myelin-forming oligodendrocytes depends on the transcription factor Sox10. Genes & development. 2002 Jan 15; 16(2):165–70. [PubMed: 11799060]
26. Zhou Q, Anderson DJ. The bHLH transcription factors OLIG2 and OLIG1 couple neuronal and glial subtype specification. Cell. 2002 Apr 5; 109(1):61–73. [PubMed: 11955447]
27. Bujalka H, Koenning M, Jackson S, et al. MYRF is a membrane-associated transcription factor that autoproteolytically cleaves to directly activate myelin genes. PLoS Biol. 2013; 11(8):e1001625. [PubMed: 23966833]
28. Werner T, Hammer A, Wahlbuhl M, Bosl MR, Wegner M. Multiple conserved regulatory elements with overlapping functions determine Sox10 expression in mouse embryogenesis. Nucleic acids research. 2007; 35(19):6526–38. [PubMed: 17897962]
29. Yu Y, Chen Y, Kim B, et al. Olig2 targets chromatin remodelers to enhancers to initiate oligodendrocyte differentiation. Cell. 2013 Jan 17; 152(1–2):248–61. [PubMed: 23332759]
30. Weider M, Kuspert M, Bischof M, et al. Chromatin-remodeling factor Brg1 is required for Schwann cell differentiation and myelination. Dev Cell. 2012 Jul 17; 23(1):193–201. [PubMed: 22814607]
31. Chen Y, Wu H, Wang S, et al. The oligodendrocyte-specific G protein-coupled receptor GPR17 is a cell-intrinsic timer of myelination. Nat Neurosci. 2009 Nov; 12(11):1398–406. [PubMed: 19838178]

32. Nogales E, Zhang R. Visualizing microtubule structural transitions and interactions with associated proteins. Curr Opin Struct Biol. 2016 Apr.37:90–6. [PubMed: 26803284]
33. Romaniello R, Arrigoni F, Bassi MT, Borgatti R. Mutations in alpha- and beta-tubulin encoding genes: implications in brain malformations. Brain Dev. 2015 Mar; 37(3):273–80. [PubMed: 25008804]
34. Zuchero JB, Fu MM, Sloan SA, et al. CNS myelin wrapping is driven by actin disassembly. Developmental cell. 2015 Jul 27; 34(2):152–67. [PubMed: 26166300]
35. Song J, Goetz BD, Baas PW, Duncan ID. Cytoskeletal reorganization during the formation of oligodendrocyte processes and branches. Mol Cell Neurosci. 2001; 17:624–36. [PubMed: 11312599]
36. Carson JH, Kwon S, Barbarese E. RNA trafficking in myelinating cells. CurrOpinNeurobiol. 1998; 8:607–12.
37. Bauer NG, Richter-Landsberg C, ffrench-Constant C. Role of the oligodendroglial cytoskeleton in differentiation and myelination. Glia. 2009 May 19.
38. Lunn KF, Baas PW, Duncan ID. Microtubule organization and stability in the oligodendrocyte. JNeurosci. 1997; 17:4921–32. [PubMed: 9185530]
39. Purnell SM, Bleyl SB, Bonkowsky JL. Clinical exome sequencing identifies a novel TUBB4A mutation in a child with static hypomyelinating leukodystrophy. Pediatr Neurol. 2014 Jun; 50(6): 608–11. [PubMed: 24742798]
40. Shen XY, Billings-Gagliardi S, Sidman RL, Wolf MK. Myelin deficient (shi-mld) mutant allele: Morphological comparison with shiverer (shi) allele on a B6C3 mouse stock. Brain Res. 1985; 360:235–47. [PubMed: 2416404]
41. Song J, Goetz BD, Kirvell SL, Butt AM, Duncan ID. Selective myelin defects in the anterior medullary velum of the taiep mutant rat. Glia. 2001 Jan; 33(1):1–11. [PubMed: 11169787]
42. Butt AM, Berry M. Oligodendrocytes and the control of myelination in vivo: new insights from the rat anterior medullary velum. J Neurosci Res. 2000 Feb 15; 59(4):477–88. [PubMed: 10679786]
43. Song J, O'Connor LT, Yu W, Baas PW, Duncan ID. Microtubule alterations in cultured taiep rat oligodendrocytes lead to deficits in myelin membrane formation. JNeurocytol. 1999; 28:671–83. [PubMed: 10851346]
44. Masurovsky EB, Peterson ER, Crain SM, Horwitz SB. taxol effects on glia in organotypic mouse spinal cord-drg cultures. Cell Biol Int Rep. 1985; 9:539–46. [PubMed: 2862999]
45. Nogales E, Grayer Wolf S, Khan IA, Luduena RF, Downing KH. Structure of tubulin at 6.5 A and location of the taxol-binding site. Nature. 1995; 375:424–7. [PubMed: 7760939]
46. Tischfield MA, Baris HN, Wu C, et al. Human TUBB3 mutations perturb microtubule dynamics, kinesin interactions, and axon guidance. Cell. 2010 Jan 8; 140(1):74–87. [PubMed: 20074521]
47. Geva M, Cabilly Y, Assaf Y, et al. A mouse model for eukaryotic translation initiation factor 2B-leucodystrophy reveals abnormal development of brain white matter. Brain. 2010 Aug; 133(Pt 8): 2448–61. [PubMed: 20826436]
48. Dooves S, Bugiani M, Postma NL, et al. Astrocytes are central in the pathomechanisms of vanishing white matter. J Clin Invest. 2016 Apr 01; 126(4):1512–24. [PubMed: 26974157]
49. Niwa S, Takahashi H, Hirokawa N. beta-Tubulin mutations that cause severe neuropathies disrupt axonal transport. EMBO J. 2013 May 15; 32(10):1352–64. [PubMed: 23503589]
50. Brouhard GJ. Dynamic instability 30 years later: complexities in microtubule growth and catastrophe. Mol Biol Cell. 2015 Apr 1; 26(7):1207–10. [PubMed: 25823928]
51. Mitchison T, Kirschner M. Dynamic instability of microtubule growth. Nature. 1984 Nov 15–21; 312(5991):237–42. [PubMed: 6504138]
52. Song J, Carson JH, Barbarese E, Li FY, Duncan ID. RNA transport in oligodendrocytes from the taiep mutant rat. Mol Cell Neurosci. 2003 Dec; 24(4):926–38. [PubMed: 14697659]

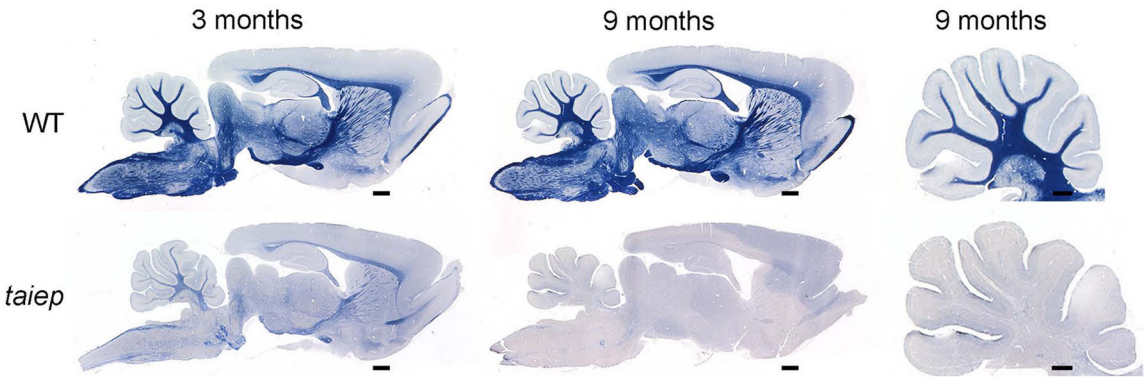

Fig. 1. Myelin is initially present though reduced in the *taiep* brain and is lost with time

There is evidence of myelin in the brain of a 3 month old *taiep* rat, noticeably in the cerebellum, corpus callosum and fornix but much less than wild type. However by 9 months, demyelination has led to severe loss of myelin. In the cerebellum there is mild separation of the gyri suggesting atrophy that may have resulted from myelin loss. Scale bars: 0.5 mm (cerebellum), 1.0 mm (whole brain).

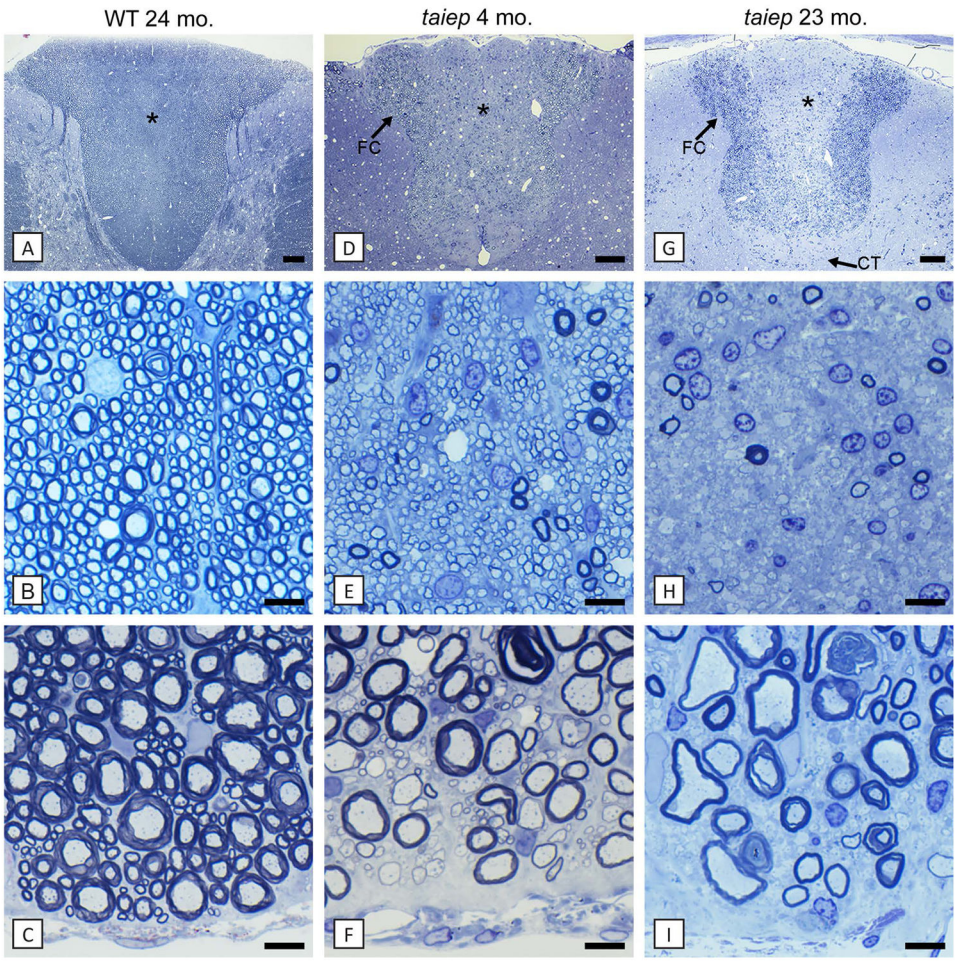

Fig. 2. In the spinal cord, the dorsal column shows both hypomyelination followed by complete demyelination of certain tracts

In the *taiep* rat spinal cord at early time points, all axons in the fasciculus gracilis (*, E) were myelinated but with thinner myelin sheaths than in controls (B). However, with time the dorsal column and particularly the fasciculus gracilis (*) and corticospinal tract (↑CT) show severe demyelination with only scattered large diameter axons being myelinated (G, H). In comparison, the fasciculus cuneatus was less severely affected (↑FC). There was an increase in glial cell nuclei in these tracts with time (H). In contrast, the ventral column from the same animals as in A-H showed that axons at 4 months were mainly thinly myelinated or non-myelinated in *taiep* and remained this way through 23 months (I). WT = wild type. Scale bars: 20 μm (B, C, E, F, H, I), 200 μm (A, D, G). (In color in online version)

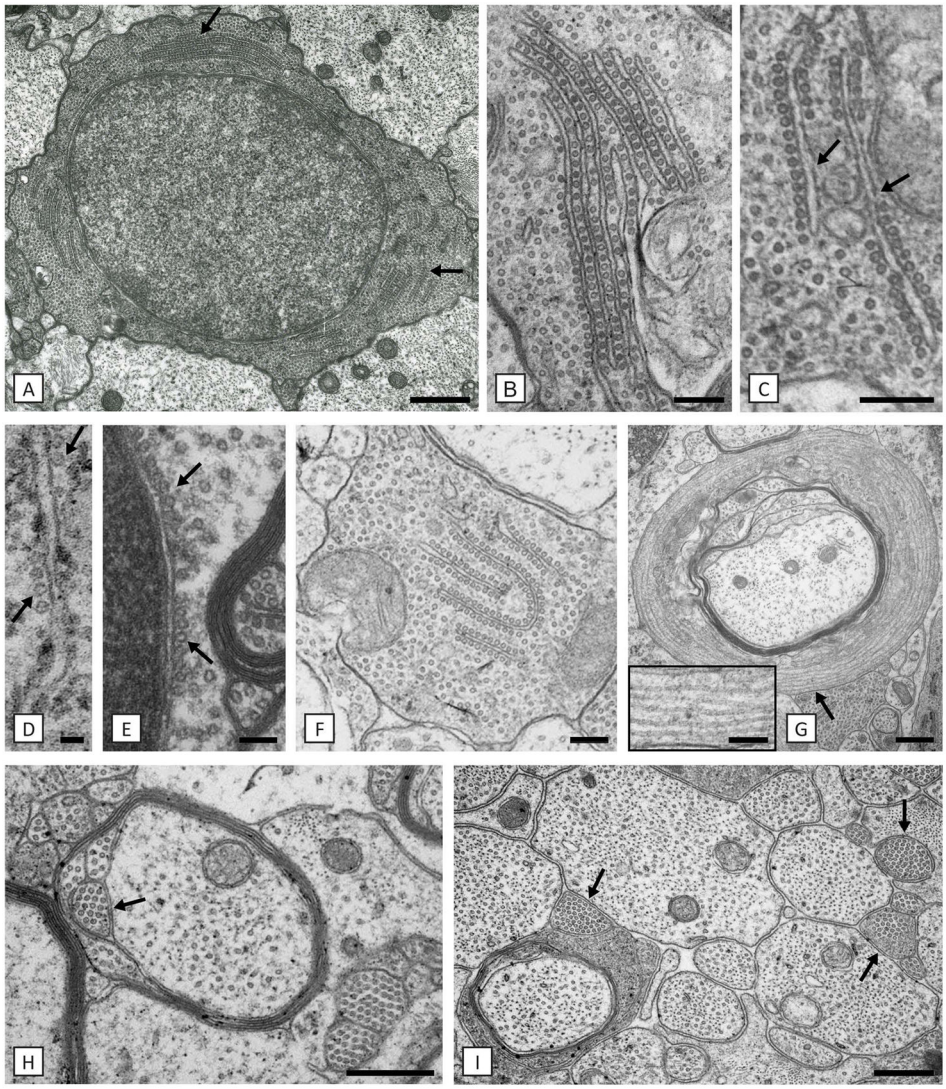

Fig. 3. Accumulation of microtubules, solely in oligodendrocytes, defines the defect

A) Oligodendrocytes contain densely packed microtubules and are often present in ER-associated arrays (arrows). On higher power, details of these arrays can be seen with microtubules linking adjacent (B) or separate (C) membranes where they appear discontinuous (C, arrows). In B) and C) there is also an increase in “free” microtubules. Microtubules also are aligned along RER and the outer nuclear membrane (D, E) (arrows). In D) the microtubules may have displaced ribosomes. F) Oligodendrocyte processes are frequently packed with microtubules that can also be aligned with ER (F). Numerous examples of excess microtubules circling myelinated axons were noted (G). High power from area ↑ shows more detail of the microtubules (G-inset). H) Collections of microtubules were frequently seen in duplicated inner loops (arrow). I) Axons of all diameters had normal density of microtubules in contrast to the adjacent oligodendrocyte ‘microprocesses’ (arrows). Scale bars: 50 nm (D), 100 nm (E), 200 nm (B, C, F, G-inset), 500 nm (A, H, I), 600 nm (G).

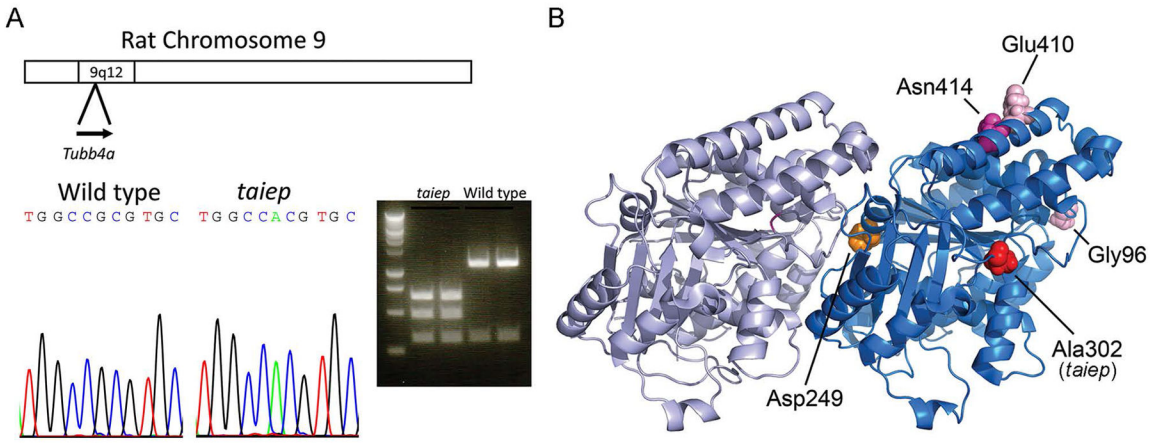

Fig. 4. Identification of *Tubb4a* mutation in *taiep* rat

A) Previous work had localized the causative gene in the *taiep* mutant to rat chromosome 9q12. Analysis of candidate genes revealed *Tubb4a*, which is mutated in several patients with hypomyelination. Sequencing of *taiep* mutant rats and normal controls revealed an A to G mutation that changes Ala302 to Thr. The mutation also introduces a MscI restriction enzyme site. PCR fragments were generated from *taiep* rat and wild type littermate cDNA, and both fragments were digested with the MscI restriction enzyme, indicating a homozygous mutation in *taiep*. B) The crystal structure of α- and β-tubulins was used to indicate the position of the Ala302 residue that is mutated in the *taiep* rat and the Asn414 residue mutated in our patient. Additionally the position of the classical H-ABC mutation (Asp249) and two other patients with isolated hypomyelination (Glu410 and Gly96) are shown. The classical H-ABC mutation is located at the α-β interface where most H-ABC mutations are located, whereas the *taiep* mutation and the mutations observed in patients with isolated hypomyelination are located at the lateral side of β-tubulin.

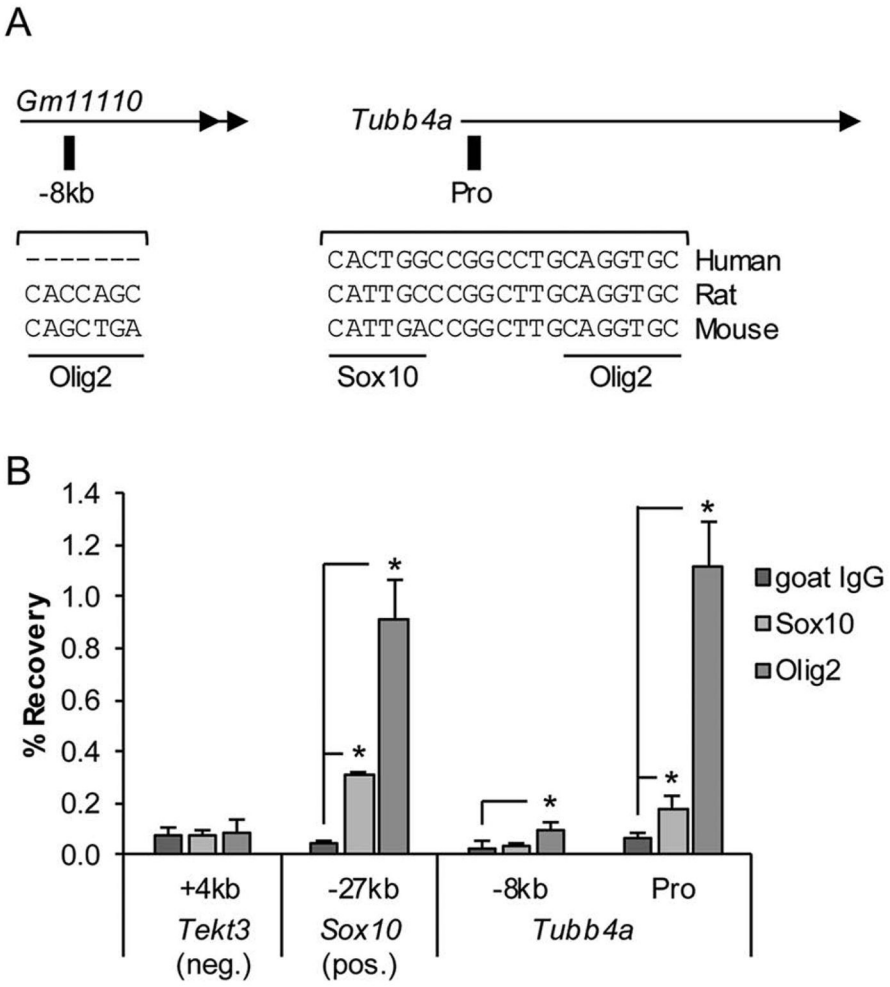

Fig. 5. Sox10 and Olig2 bind the *Tubb4a* gene promoter

A) Schematic shown depicts location of genomic regions assayed by ChIP. Sox10 and Olig2 binding motifs are indicated and sequences are compared between species. Note that the motifs vary in relation to the consensus motifs for each: C(A/T)TTGT for Sox10 and CAGCTGC for Olig2. Also, the region at −8kb is not very conserved and the Sox10 motif near the gene promoter (Pro) is not conserved in humans. *Gm11110* is a predicted long noncoding RNA annotated in the mouse genome build mm10. B) ChIP-qPCR analysis identifies Sox10 and Olig2 binding in P15 mouse thoracic spinal cord. Genomic regions assayed are listed on the x-axis with respect to the given gene translation start site and includes a negative control site within the *Tekt3* gene and a positive control site −27kb upstream of *Sox10*. At each site, percent recoveries for Sox10 or Olig2 ChIP were compared with that of a control IP (goat IgG). Error bars represent the standard deviation of three independent experiments (*p<0.05).

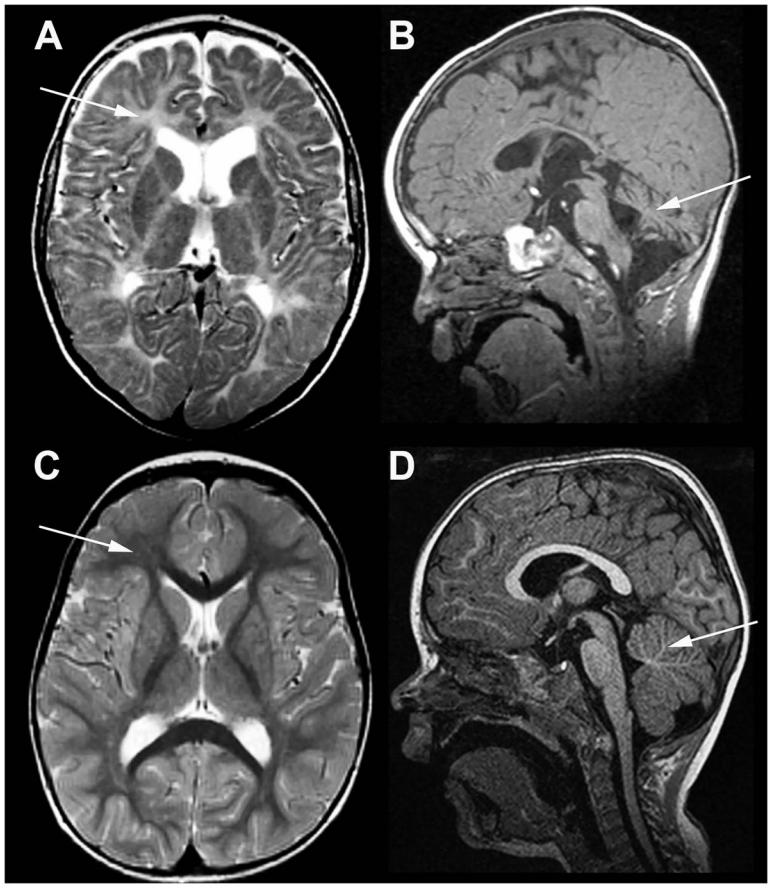

Fig. 6. MRI in the patient with *TUBB4A*-related severe hypomyelination and atrophy of the cerebellum

A, B) T2-weighted axial (A) and T1-weighted sagittal (B) images of the patient obtained at the age of 2½ years; C, D, same images of an age-matched neurologically normal child. In the patient the cerebral white matter is T2-hyperintense due to lack of myelin (arrow in A), while the white matter in the control is T2-hypointense (arrow in C). In the patient the cerebellum is mildly atrophic (arrow in B), while it is normal in the control (arrow in D).

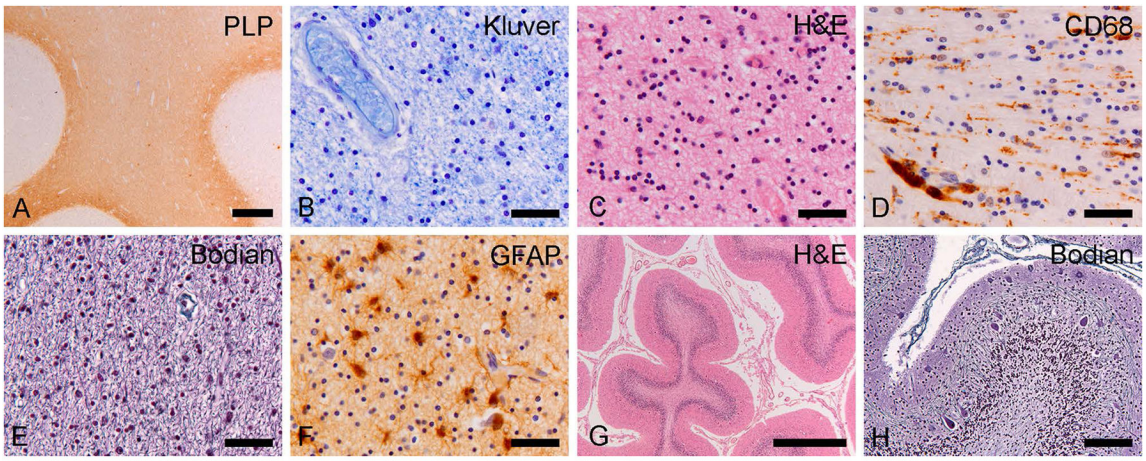

Fig. 7. Neuropathology of the patient with *TUBB4A*-related severe hypomyelination and atrophy of the cerebellum

A) Proteolipid protein (PLP) stain for myelin of the frontal lobe shows lack of white matter myelin with relative preservation of the U-fibers. B) Klüver stain for myelin shows profound lack of myelin in the deep white matter of the parietal lobe. C) At high magnification, the number of white matter oligodendrocytes (cells with small, compact, round nuclei and a clear perinuclear halo) appears increased on this H&E-stained section of the parietal lobe. D) CD68 stain for microglia/macrophages shows activation of microglia in the temporal white matter with clustering of macrophages around blood vessels. E) Bodian stain for axons shows axonal preservation in the temporal lobe white matter without axonal varicosities or spheroids. F) Stain against the astrocyte-specific glial fibrillary acidic protein (GFAP) shows moderate reactive astrogliosis in the frontal white matter. G) H&E stain of the cerebellum shows enlargement of the sulci and thinning of the cortex with loss of neurons in the molecular layer. H) Bodian stain of the cerebellar cortex shows mild drop out of Purkinje cells and presence of Purkinje cell dendritic swellings in the molecular layer. Scale bars: 20 μm (B–F), 40 μm (H), 500 μm (G), 1 mm (A).

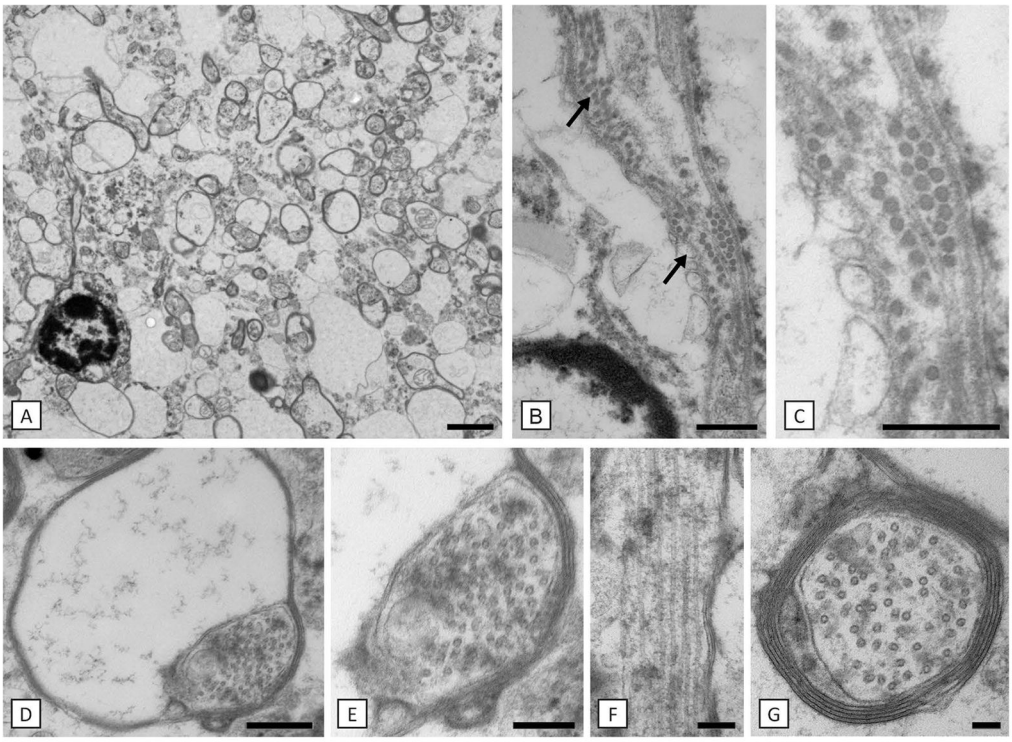

Fig. 8. Hypomyelination is associated with microtubule accumulation in the patient

Axons are either non-myelinated or have thin myelin sheaths (A). Close to a putative oligodendrocyte nucleus there are rows of microtubules (arrows in B). Magnification of one of these areas is shown in C). The most distal part of the oligodendrocyte process, the inner loop is enlarged and filled with microtubules (D, E). An oligodendrocyte process seen on longitudinal section contains prominent microtubules (F). Microtubules were also prominent in myelinated and non-myelinated axons (G). Scale bars: 100 nm (G), 200 nm (E, F), 400 nm (C, D), 500 nm (B), 2 μm (A).